Pegmatites as geological expressions of spontaneous crustal flow localisation

Alexis Plunder, Laetitia Le Pourhiet, L. Räss, Eric Gloaguen, Michel Pichavant, Charles Gumiaux

▶ **To cite this version:**

Alexis Plunder, Laetitia Le Pourhiet, L. Räss, Eric Gloaguen, Michel Pichavant, et al.. Pegmatites as geological expressions of spontaneous crustal flow localisation. Lithos, 2022, 416-417, pp.106652. 10.1016/j.lithos.2022.106652 . hal-03666402

HAL Id: hal-03666402
https://brgm.hal.science/hal-03666402

Submitted on 12 May 2022

HAL is a multi-disciplinary open access archive for the deposit and dissemination of scientific research documents, whether they are published or not. The documents may come from teaching and research institutions in France or abroad, or from public or private research centers.

L'archive ouverte pluridisciplinaire **HAL**, est destinée au dépôt et à la diffusion de documents scientifiques de niveau recherche, publiés ou non, émanant des établissements d'enseignement et de recherche français ou étrangers, des laboratoires publics ou privés.

Distributed under a Creative Commons Attribution - NonCommercial - NoDerivatives 4.0 International License

LITHOS 416-417 (2022) 106652

Contents lists available at ScienceDirect

LITHOS

journal homepage: www.elsevier.com/locate/lithos

Pegmatites as geological expressions of spontaneous crustal flow localisation

A. Plunder [a,b,*], L. Le Pourhiet [a], L. Räss [c,d], E. Gloaguen [b,e], M. Pichavant [e], C. Gumiaux [e]

[a] Sorbonne Université, CNRS-INSU, Institut des Sciences de la Terre Paris, ISTeP UMR 7193, 75005 Paris, France
[b] BRGM, F-45060 Orléans, France
[c] Laboratory of Hydraulics, Hydrology and Glaciology (VAW), ETH Zurich, Zurich, Switzerland
[d] Swiss Federal Institute for Forest, Snow and Landscape Research (WSL), Birmensdorf, Switzerland
[e] Université d'Orléans/CNRS/BRGM/ISTO, UMR 7327, F-45071 Orléans, France

ARTICLE INFO

Keywords:
Pegmatite
Partial melting
Two-phase flow
Porosity waves
Numerical modelling

ABSTRACT

Amongst the silicate-rich crystalline rocks that are produced in the continental crust, pegmatites are characterised by their large crystals which give them both an aesthetic and economic interest. Pegmatites crystallise either from fractionated magma derived from a parent granitic body or from the partial melting of meta-sediments or meta-igneous rocks (e.g. amphibolite). The mechanism of residual magma (or fluid) extraction from the parent granitic body has been thoroughly studied, but pegmatitic melt extraction after partial melting has received less attention. We present here a series of non-dimensional numerical experiments using a two-phase flow formulation that couples the Stokes problem to/with non-linear Darcy flow. This approach makes it possible to predict the movement of fluid inclusions (named porosity) in a deformable of a viscous rocks (named porous matrix). We find that the simulation produces either clusters or an isolated body of fluid inclusion depending on the compaction/decompaction ratio of the effectively viscous matrix in which they rise. Using a review of pegmatite natural properties, we propose a scaling of our numerical simulations that describes the ascent of a pegmatite-forming melt produced by partial melting. We then discuss possible travel distances and temperature effects. To discuss our results in light of field observations, we assume that the compaction-decompaction ratio is an accurate proxy for the influence of brittle processes at a scale smaller than the representative volume element, and therefore corresponds structural level variations at which pegmatites are emplaced. We find that our numerical simulation explain the statistical organisation, in terms of level of emplacement, of real fields of pegmatites possibly derived from partial melting of meta-sediments. Pegmatites in fact tend to organise as clusters around brittle faults in upper crustal levels, whereas they present a scattered distribution at mid to lower crustal levels. Our results therefore show that porosity waves are a possible mechanism for rapidly extracting and transporting pegmatite melts formed during low-degree (ca. 10%) partial melting at distances up to a few kilometres in the crust.

1. Introduction

Pegmatites are igneous rocks that are generally of granitic composition. They are characterised by extremely coarse but variable grain size and by specific crystal growth texture (e.g. skeletal crystals or any strongly directional growth habits; London, 2018). Due to their crystal size, pegmatites produce amongst the purest minerals used in the ceramic industry. Locally, they can also be enriched in rare elements (e.g. Li, Ta, Sn, Cs, Be, REE amongst others). In nature, pegmatites form fields observed at various crustal levels (mid-lower to upper levels). Granitic pegmatites are thought to crystallise either from extremely fractionated granitic magma expelled at the end of the evolution of large granitic bodies (the "Cameron" or differentiation model; Cameron et al., 1949; Černý et al., 2005) or from melts generated by partial melting of meta-sediments (the "Stewart" or anatectic model; (e.g. Fei et al., 2020; Gourcerol et al., 2019; Müller et al., 2015; Müller et al., 2017; Simmons and Webber, 2008; Stewart, 1978; Webber et al., 2019). In addition to their occasional rare-element enrichment, pegmatites also contain abundant volatile elements (H_2O, F, B, P). In the differentiation model, this geochemical specialisation is attributed to the progressive evolution

* Corresponding author at: Sorbonne Université, CNRS-INSU, Institut des Sciences de la Terre Paris, ISTeP UMR 7193, 75005 Paris, France.
E-mail address: a.plunder@brgm.fr (A. Plunder).

https://doi.org/10.1016/j.lithos.2022.106652
Received 6 September 2021; Received in revised form 17 December 2021; Accepted 28 February 2022
Available online 7 March 2022
0024-4937/© 2022 The Authors. Published by Elsevier B.V. This is an open access article under the CC BY-NC-ND license (http://creativecommons.org/licenses/by-nc-nd/4.0/).

of residual magma as quartz and feldspar crystallization proceeds (e.g. Cameron et al., 1949; Černý et al., 2005; London, 2018). Alternatively, in the anatectic model, low degrees of partial melting and the bulk rock composition of source rocks control pegmatite chemistry (Barros and Menuge, 2016; Demartis et al., 2011; Fei et al., 2020; Gourcerol et al., 2019; Müller et al., 2017; Simmons et al., 2016; Stewart, 1978; Webber et al., 2019). Both the differentiation and anatectic models are considered valid for the generation of barren pegmatites (Černý and Ercit, 2005; Simmons and Webber, 2008). There is however an ongoing debate concerning the genesis of rare-metal pegmatite especially in places where granite is not observed in the vicinity of the ore-bearing pegmatite. Yet, a handful of authors consider that the anatectic model is geochemically valid to explain rare metal pegmatite in certain location (e.g. Müller et al., 2017; Shaw et al., 2016; Webber et al., 2019).

In a few places, the anatectic model offers a better explanation for the field and structural characteristics of pegmatite fields than the differentiation model. Various orogenies provide different examples of the relationship between pegmatite fields and anatectic areas (Deveaud et al., 2013; Müller et al., 2017; Silva et al., 2018). These examples are observed in the Variscan, Sveconorwegian, Svecofennian orogenies and the Appalachian belt where (i) pegmatites are not genetically related to the surrounding granite intrusions (e.g. Simmons and Webber, 2008) and (ii) a pegmatite field is emplaced without a granitic source (Demartis et al., 2011; Melleton et al., 2012; Müller et al., 2017; Webber et al., 2019).

Spatial statistical analysis on different pegmatite fields located in the European Variscan belt and more precisely in the French Massif Central (Limousin and Montagne Noire), and in the Cap de Creus (Spain) suggest that anatectic pegmatite distribution is directly related to the host rock; pegmatites cluster along brittle faults in upper crustal levels and are scattered at deeper crustal levels (Fig. 1; Deveaud et al., 2013). This unusual geometric distribution provides an important opportunity to validate models of extraction and ascent of pegmatitic melts of anatectic origin.

Previous attempts to model anatectic pegmatite emplacement were based on Darcy flow coupled with heat advection-diffusion models (Deveaud et al., 2015). However, pegmatite melts have physical properties that differ from hydrothermal fluids and connected porosity if present, is low at the depths considered for pegmatite extraction and emplacement. In addition, if these models do produce thermal solitons, their diffusive behaviour does not provide a mechanism that could produce the clustering observed in the upper crust and in the vicinity of lithological contrasts or faults. Pegmatite melts must be emplaced rapidly enough to preserve thermal contrast with host rocks, which is the condition for the development of their characteristic textures (e.g. Devineau et al., 2020; London and Morgan, 2017). This observation raises the question: How do small melt pods travel rapidly enough and do not cool? Fast fluid/melt velocity at crustal levels would require high crustal permeability and low fluid viscosity. "Dynamic permeability" (i.e. the ratio of static permeability to fluid viscosity) is here well suited to studying pegmatite emplacement processes. Rapid travel would result in locally high effective (dynamic) permeability values of/in the crust.

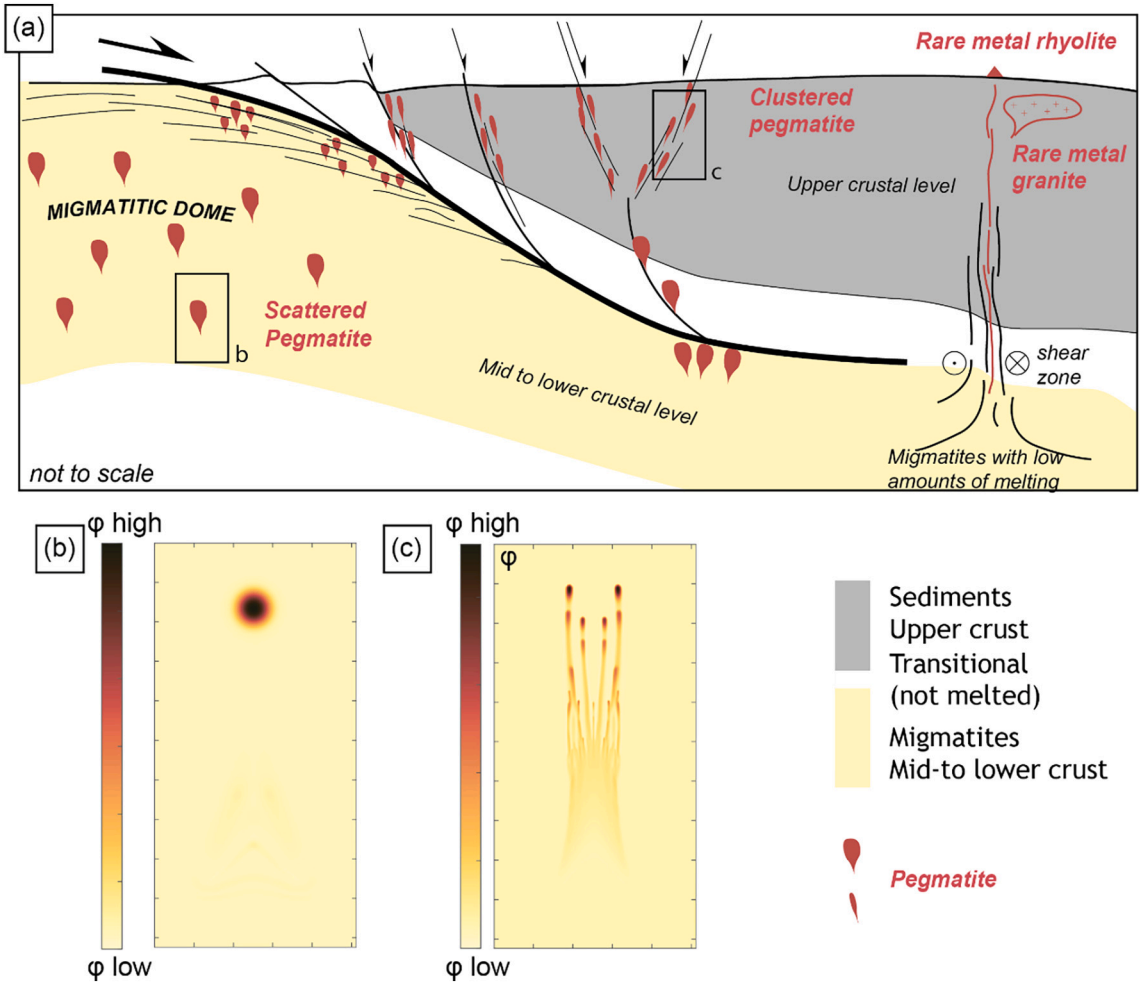

Fig. 1. (a) Schematic geological cross section of a post-collisional setting showing the development of a migmatitic dome (modified after Gourcerol et al. (2019); (b) Porosity field φ of a two-phase flow simulation in a purely viscous rheology; (c) Porosity field φ of a two-phase flow simulation in a visco-plastic rheology.

These values are much higher than those measured in the laboratory and closer to values observed in fault zones (e.g. Duwiquet et al., 2019).

A clustering pattern similar to that observed in pegmatite fields, is well described by the geometry of porosity waves that form in fluid -saturated porous environments such as sedimentary stacks (e.g. Räss et al., 2018; Räss et al., 2019). Solitary waves of porosity are the result of coupled hydromechanical processes that lead to the spontaneous formation of localised highly permeable flow paths. The dynamic increase of effective permeability in the crust produces orders-of-magnitude faster vertical fluid ascent rates compared to single-phase Stokes flow or diffusive Darcy flow. This approach has been successfully applied to explain kimberlite ascent (Connolly and Podladchikov, 2007) and intra-arc magma transport (Bouilhol et al., 2011), with potential application to anatectic melt extraction (Brown, 2013).

Here we use numerical models of coupled hydromechanical processes to investigate how small bodies of pegmatitic melt can rapidly migrate through a crustal section. We first present a short review of pegmatites properties. We then present the different strategies for fluid transport modelling in geosciences. The second part of the present work is dedicated to model results and scaling with application to pegmatites. We discuss the physical quantities such as pegmatitic melt viscosity, crustal viscosity values, and the effective permeability of migmatite that match the conditions leading to the development of porosity waves. Since we do not consider thermal coupling effects in our model we use an a posteriori assessment that confirms that melt bodies do not significantly cool during their ascent. We finally discuss the implications of our models, (i) in light of granitic pegmatite genesis throughout anatexis and during emplacement, (ii) compare with available field observation for both barren and rare metal bearing pegmatite and (iii) consider the limitation of our modelling approach.

2. Pegmatites and their properties

As already introduced, pegmatites are igneous rocks of a generally granitic composition that are characterised by extremely coarse and variable crystal size. We refer the reader to London (2018) or to Simmons and Webber (2008) and references therein for a more extensive review of pegmatites and their characteristics. We here recall the essential parameters for our application, that is, melt viscosity during extraction and ascent and its crystallization temperature.

Pegmatite melt viscosity has been studied experimentally (2013, 2011; Bartels et al., 2015) or extrapolated from the composition of melt inclusions (Thomas and Davidson, 2012). The viscosity of a silicate melt can be predicted from its bulk composition (Giordano et al., 2008). The bulk chemistry of a pegmatite is more complex to evaluate than that of a granite or rhyolite because its crystals are larger. The complex texture of pegmatites induces or reflects significant spatial variation in chemical composition. Generally, it the composition is averaged from thousands of bodies or from fine-grained cogenetic aplite and typically compares to a rhyolite composition (London, 2018), such as the Macusani glass (Pichavant et al., 1987). Experimental petrology and melt inclusion measurement gives only imprecise constraints on pegmatitic melt viscosity, which can range from 1 to 10^{14} Pa.s depending on the melt chemistry, the temperature, and the amount of water or other flux elements such as Li or F (Bartels et al., 2013, 2011; Bartels et al., 2015; Thomas and Davidson, 2012). These constraints are largely related to the variable amount of water contained in a pegmatite melt (from a few weight % to about 20 wt%). This issue constitutes an open debate in the community (London, 2015; Thomas and Davidson, 2012). Assuming that pegmatite texture can be reproduced experimentally with reasonable quantities of water (5–10 wt%; Devineau et al., 2020) lowers the possible viscosity to a few log units around an average of 10^4 Pa.s at a temperature of 600 °C.

Experimental work also shows that a critical parameter that enables pegmatites to acquire their specific texture is crystallization in an undercooled state (Devineau et al., 2020; London and Morgan, 2017). This means that they travel as a liquid (at ca. 650 °C, a reasonable temperature for the liquidus) and crystallise when they encounter wall rocks at temperatures ca. 100–200 °C below their liquidus. Moreover, volcanic systems suggest that the temperature loss during rapid melt ascent is probably minor and therefore negligible (Myers et al., 2019). We therefore assume that the temperature of the pegmatitic melt does not significantly change during transport. This important assumption implies a constant pegmatite melt viscosity during ascent.

Pegmatite crystallization temperature is generally hard to measure because most classical geothermometers are often not applicable (e.g. Ti in quartz, muscovite or biotite; see London, 2014). Nevertheless, two-feldspar thermometry, when applicable, suggests temperatures of 450 ± 50 °C (London, 2018). Oxygen isotopes on various minerals (e.g. quartz-tourmaline) give temperatures in the range 450–600 °C (e.g. London, 2018 and references therein). Titanium in quartz, when carefully applied, gives a similar temperature range and is a powerful tool (Müller et al., 2015). These temperatures are compatible with the solidus temperature reported during experiments on the most fractionated and Li-rich liquids (London et al., 1989) and of water-saturated haplogranitic composition (Devineau et al., 2020).

Pegmatite cooling has been investigated using both experimental petrology and numerical models. Both methods demonstrate that pegmatite bodies cool rapidly. Numerical models by Chakoumakos and Lumpkin (1990) show that the cooling of a 20 m thick dyke in a host-rock at 550 °C would take place in ~100 yrs. Trace-element advection diffusion modelling suggests that decimetre-sized pegmatite can form within a timescale of days (Phelps et al., 2020).

3. Fluid transport modelling in geosciences

This section briefly compares different approaches of fluid transport modelling in geosciences.

We emphasize that understanding the transport of the pegmatite-forming melt in the crust is not yet fully understood, nor is the ability of a pegmatitic melt to be transported over kilometres. Rubin (1995) argues that granitic dykes are unlikely to migrate beyond the thermal aureole surrounding granitic bodies because they will freeze as soon as they encounter host rock below the melt solidus. Baker (1998) argues that pegmatitic melt can migrate in a dyke as far as 10 km if the plutons exceed dimensions of 10 km^3 or if open fractures are present prior to the propagation of the melt. Such fractures imply the presence of a constant/infinite magma source during a short-lived period during the late stages of granite crystallization (Rubin, 1998). Finally, this mechanism applies only in the presence of a large concentration of melt-filled cracks (i.e. a granitic pluton); it cannot explain spontaneous generation of a pegmatite field from a rock in which the melt is pervasively distributed (i.e. during anatexis).

Yarushina et al. (2015) conducted a thorough review of the various modelling strategies used to model flow in porous media during the last century. The choice of strategy largely depends on the scale of the representative volume element considered. We summarise them below and in Fig. 2. Hydrogeology generally considers the application of the empirical Darcy law where a constant fluid flow passes through a porous matrix (Hiscock and Bense, 2014). It applies to laminar flow and does not take pore geometry into account (Fig. 2a). Fluid velocity is constant. However, at the microscopic scale, the fluid follows non-rectilinear streamlines, introducing a complexity of the material: the so-called tortuosity. One approach is to consider the solid as fixed and to calculate the effective trajectories of the fluid in the porous media using momentum and mass continuity equations for the fluid (Fig. 2b).

When heat transfer is coupled to Darcy's law through temperature-dependent density and viscosity, buoyancy effects may significantly affect the velocity field and create independent plumes (or blobs) of rising fluids with anomalously high velocity (Deveaud et al., 2015).

For geological problems (e.g. crystal mush in a magma)), the solid phase can move within the fluid. Processes considering both the motion

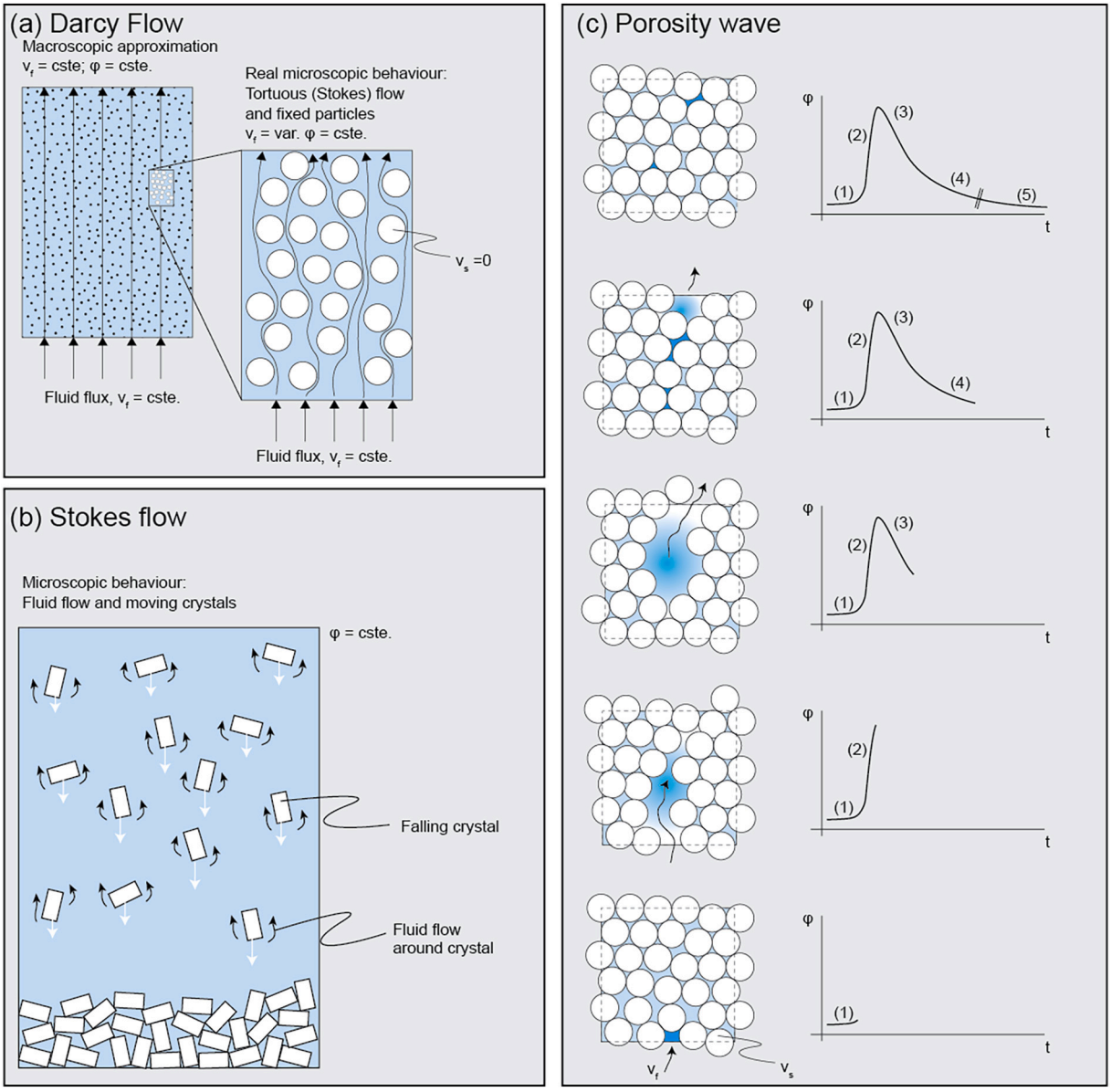

Fig. 2. Illustration of the principal methods to simulate fluid flow in geosciences. When present, φ denotes the porosity, v_f the fluid velocity, v_s the velocity of the solid medium, and t the time.

of solid crystals and viscous magma need to be considered. Direct numerical simulation of multi-phase flow in the suspension flow limit was proven to work efficiently but is limited to small domains: at the thin section scale, or for metre-sized dykes (Deubelbeiss et al., 2011; Yamato et al., 2015).

To resolve magma transport at the crustal or lithospheric scale, a viscous two-phase flow formulation was proposed (Keller et al., 2013; McKenzie, 1984; Räss et al., 2018; Räss et al., 2019; Schmeling et al., 2019; Scott and Stevenson, 1984; Yarushina and Podladchikov, 2015). The two-phase formulation considers the interaction of a low-viscosity 'pore' fluid in a higher viscosity 'matrix fluid', the host rock. The fractions of low and high viscosity fluids define the effective porosity of the two-phase medium. Two-phase flow combines non-linear Darcy flow and Stokes flow that describe pore-fluid motion and porous-matrix deformation, respectively. Effective pressure, the pressure difference between the total pressure – the mean stress – and the pore fluid pressure, activates local creep of the viscous matrix leading to advection of pore-space with the fluids it contains. This opening and closing results in a power-law relationship between effective porosity and permeability that fosters the development of instabilities referred to as solitary waves of porosity, or porosity waves. This mechanism describes a region of elevated pore fluid content that migrates upwards under buoyancy forces through local deformation of the surrounding porous matrix. In this way, porosity is advected with the fluid it contains. This process provides an efficient mechanism for melt transport in the mantle, for fluids expelled in sedimentary basins, or for melt migration in the crust (e.g. Connolly and Podladchikov, 2007; Connolly and Podladchikov, 2015; Keller et al., 2013; Schmeling et al., 2019; Scott and Stevenson, 1984; Yarushina et al., 2015). The transport pattern produced by this mechanism has been described to range from a single diffuse blob (Darcy flow limit) to clusters of channels with a transition consisting of a single focussed channel (Räss et al., 2019). These patterns relate directly to the asymmetry of compaction versus decompaction rates of porous media (i.e. the host rock). Rock compaction expresses as viscous deformation whereas decompaction consists of a combination of viscous deformation and grain boundary opening (Connolly and Podladchikov, 2007). This leads to the expression of bulk viscosity as follows $\eta \sim \mu_s/\varphi$ (with μ_s the shear viscosity of the rock and φ its porosity/melt content). Moreover,

grain boundary opening is sensitive to effective pressure. This effective pressure dependence of η enables rapid propagation of channelized (and clustered) flow as decompaction rates are significantly enhanced compared to compaction rates, a mechanism called decompaction weakening (Connolly and Podladchikov, 2007). The outcome, even though qualitative, relates to what is observed in nature in pegmatite fields (Fig. 1).

We propose to study whether this two-phase flow mechanism is a valid transport mode for pegmatitic melts given the scale and geometric distribution of natural pegmatitic bodies and existing experimental constraints on pegmatitic melt viscosity.

4. Results and scaling

4.1. Modelling approach

We resolve the coupled two-phase flow equations (Yarushina and Podladchikov, 2015) using the iterative and matrix-free solving strategy developed by Räss et al. (2019). We consider the two-phase flow to consist of a deforming porous medium and a Newtonian fluid. The 2D numerical experiments optimally leverage the parallel computing capabilities of an Nvidia GTX 1080 graphical processing unit, on which we performed all calculations using single-precision arithmetic. The model domain consists of a column of rock with a background porosity of 1% and includes an elliptical region with 10% porosity located at the bottom (Fig. 3). The porosity-dependent effective permeability follows a Kozeny-Carman relation in the form $k = k_0(\varphi/\varphi_0)^3$ (Costa, 2006). We applied free-slip boundary conditions for the Stokes problem. For the fluid-flow problem, we impose the flux boundary conditions to be equal to zero in the horizontal x-direction, and the effective pressure to be equal to zero (Pe = 0) on the inflow and outflow horizontal boundary of the model domain. The fluid-saturated rock column undergoes progressive viscous compaction due to downward pointing gravity acceleration. We take the fluid density to be half the solid density. We investigated the system for different values of decompaction weakening, R, a rheological constant quantifying the ratio of compaction bulk viscosity (η_C) to decompaction bulk viscosity (η_D) (Connolly and Podladchikov, 2007; Räss et al., 2018). Large values of R (significant decompaction weakening) mimic the enhanced plastic behaviour of the porous medium. Throughout all numerical experiments we used a grid resolution of 511 and 1023 cells in the x and y direction, respectively, and converged the coupled nonlinear hydromechanical problem to an absolute nonlinear tolerance of 10^{-4} allowing a stable solution (Räss et al., 2019). Non-dimensional experiments use the three scaling relations reported in Table 1: characteristic length scale or compaction length, δ_C (Connolly and Podladchikov, 2007; McKenzie, 1984); characteristic pressure (P_c); and characteristic time (τ_c) as follows: $\delta_c = \sqrt{\eta\, k/\mu_f}$, $P_c = \Delta\rho g\, \delta_c$, $\tau_c = \eta/P_c$ and their direct combination $\nu_c = \delta_c/\tau_c$.

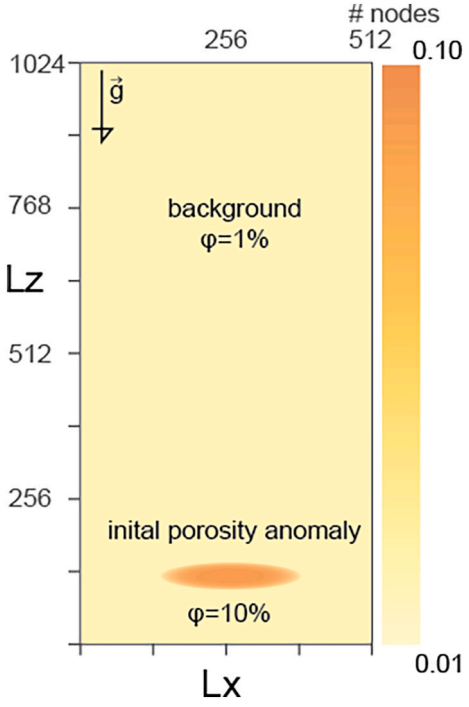

Fig. 3. Initial model configuration depicting the high porosity anomaly in the lower part and the number of grid cells as axes.

5. Results

We present two sets of non-dimensional experiment results referred to as configurations 1 and 2. The differences reside in 1) the initial non-dimensional value of dynamic permeability k/μ_f (Table 1), and 2) variations of the rheological constant R from 1 to 100 for both experiments 1 and 2.

To reflect shear strength variation of the rocks, which arises from the stacking of various tectonic units in the basement and is often associated with increased pegmatite clustering, we ran one additional experiment including a variable shear viscosity distribution featuring bands that have shear viscosity that is one order of magnitude higher than the background value ($\mu_{s1} = 10\ \mu_{s0}$). We present these results in Figs. 4 and 5. We also present a compilation of different parameters for all non-dimensional simulations in Fig. 6.

5.1. Configuration 1

For $R = 1$, we observe that porosity rapidly reaches 45% in a circular-shaped blob. A small secondary wave tends to form with the porosity that remains from the original anomaly (Fig. 4a). The three blobs rapidly merge into a single blob in the middle of the experiment, re-using the channel developed by the first wave. For $R = 10$, we observe that the porosity wave rapidly divides in two primary blobs with a maximum porosity value of 35%. Smaller blobs tend to develop and to re-use the channels previously developed by the first wave, as shown by the arrow (Fig. 4b). The secondary blob that developed in the middle of the original anomaly splits into the two main channels. The sides of the channels (or the channel walls) show a dramatic decrease in effective permeability (Räss et al., 2018). For $R = 100$, multiple channels develop from the beginning of the simulation (Fig. 4c). Porosity values rapidly reach 25%. The channel sides also show a dramatic permeability drop. Some secondary porosity waves re-use previously-formed channels. Others develop their own channels before migrating into a former channel that has higher than background effective permeability.

Adding shear viscosity variations μ_s to the initial configuration results in increased porosity wave width when it reaches a region of higher shear viscosity (Fig. 4d). Interestingly, the μ_s anomalies reduce channel spacing, allowing more interactions between new and old channels in the middle of the experiment. Maximal porosity values reach about 20%

Table 1
Non-dimensional simulation parameters.

Description	Configuration	1	2
Bulk viscosity	η	1	1
Horizontal dimension	Lx	320δc	320δc
Vertical dimension	Ly	2 Lx	2 Lx
Ref. Permeability over fluid viscosity	k/μf	0.01	0.1
Fluid density	ρf	1	1
Solid density	ρs	2	2
Characteristic lenght	δ_C	0.1	0.32
Characteristic pressure	Pc	0.1	0.32
Characteristic time	τc	10	3.2
Characteristic velocity	νc	0.01	0.1

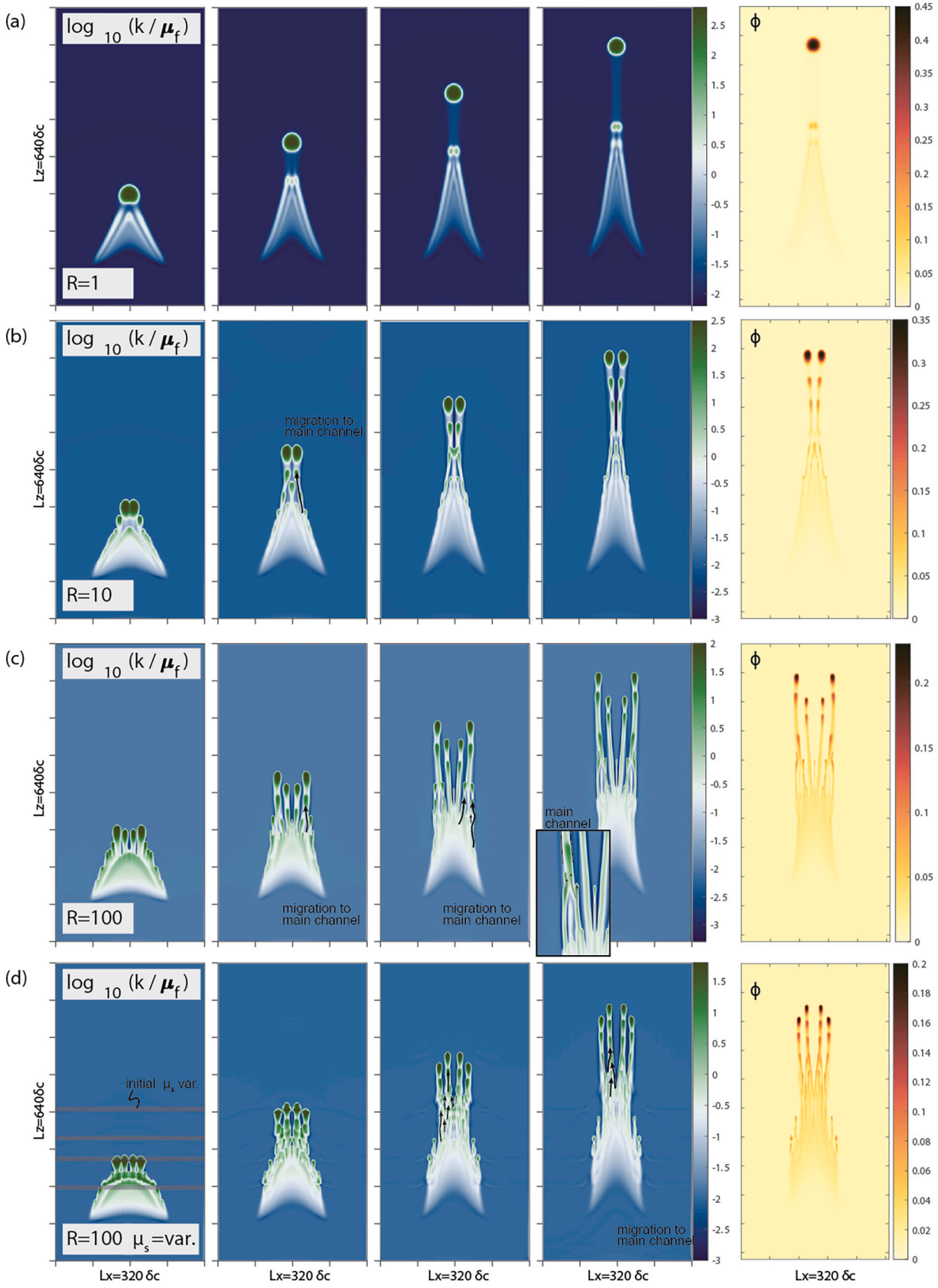

Fig. 4. Results of the numerical experiments for configuration 1 ($k/\mu_f = 0.01$). Each line (a, b, c, d) depicts a different R parameter and a specific colour axis. Note the modified initial configuration for (d) where we added horizontal perturbations in the initial shear viscosity μ_s distribution.

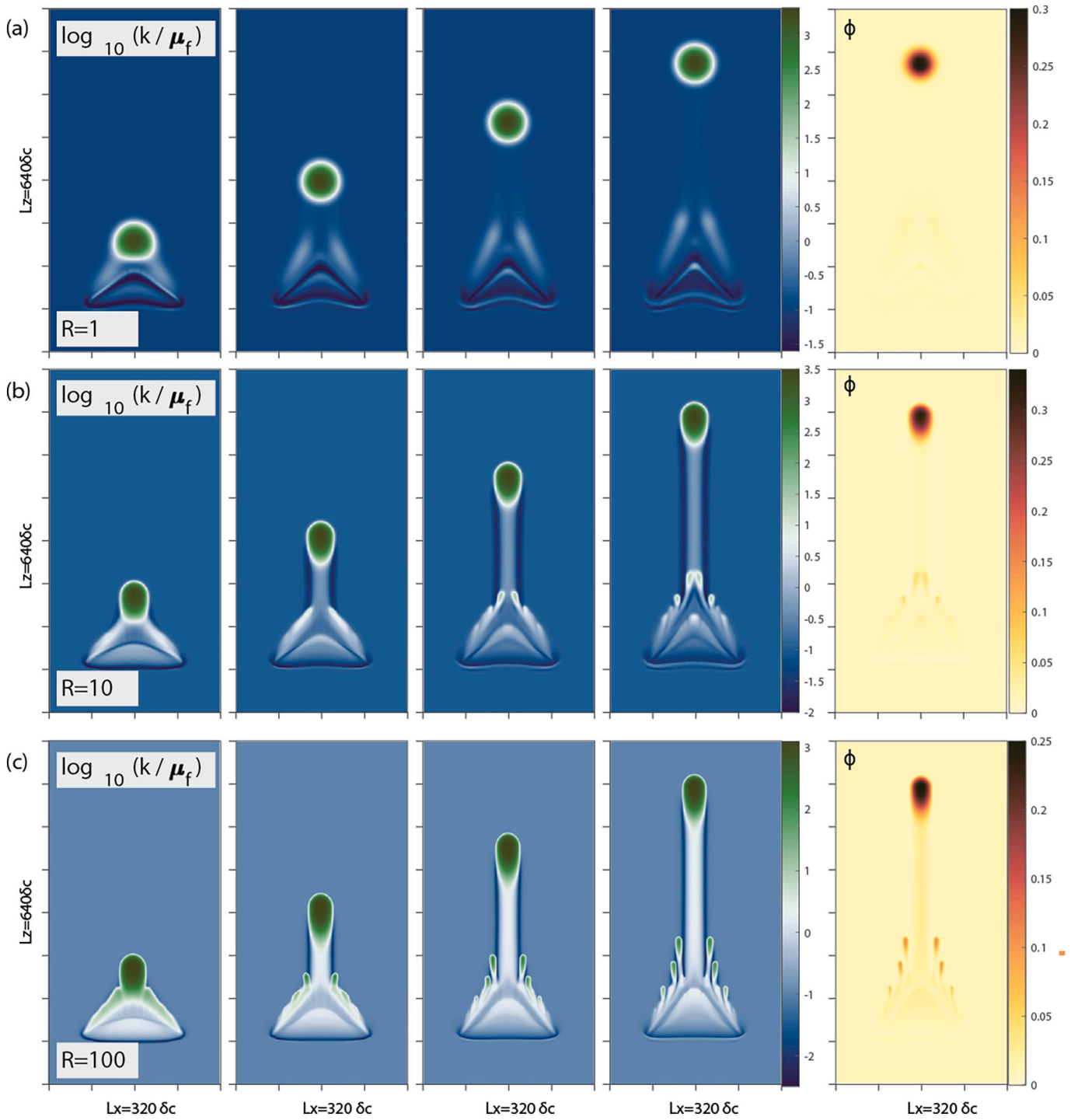

Fig. 5. Results of the numerical experiments for configuration 2 ($k/\mu_f = 0.1$). Each line (a, b, c) depicts a different R parameter and a specific colour axis.

in this layered simulation.

We note that the maximum porosity value in the experiments decreases with the increasing number of channels, because of flow rearrangement. The porosity value decreases from 45% in the experiment with R = 1 to 23% in the experiment where $R = 100$. We also point out that channel width decreases as R increases (Fig. 6a). Similar behaviour has been observed by Connolly and Podladchikov (2007). We observe a decrease in wave velocity with increasing number of channels when channel clustering occurs (Figs. 4.b,c,d and 6). The permeability contrast between channel walls and main blobs spans over 4 orders of magnitude.

5.2. Configuration 2

Note that the scale in the configuration 2 experiment is larger than that of configuration 1 (by a factor $\sqrt{10}$; see Table 1). All experiments in configuration 2 present a similar pattern, with variations in the parameter R: one principal porosity wave develops from the initial anomaly allowing smaller secondary waves to develop behind (Fig. 5a). With R = 1 we observe that porosity rapidly reaches 30% and concentrates in a circular blob (Fig. 5a). The main difference for the R = 10 configuration is that parts of the secondary waves are collected in the main channel (Fig. 5b), while for R = 100, the secondary waves never

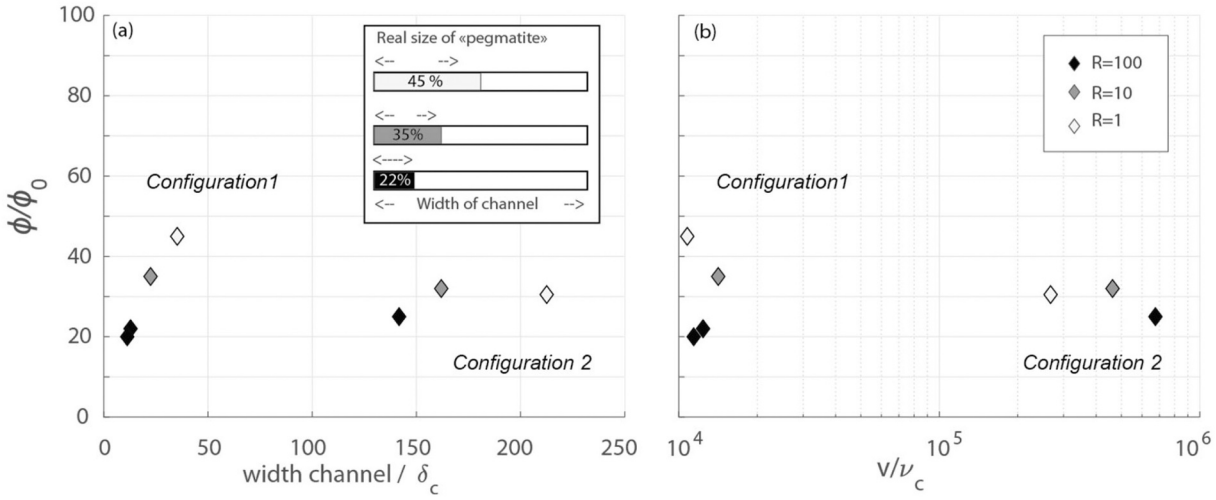

Fig. 6. Non-dimensional results of the experiments. (a) Normalised porosity as a function of channel width normalised by the characteristic compaction length. The inset compares the physical width of the melt present (i.e. corresponding to the size of a single or multiple smaller pegmatites) with respect to the channel width; (b) Normalised porosity as a function of velocity normalised by its characteristics.

collect in the main channel (Fig. 5c).

As for configuration 1, we observe that the channel width decreases with increasing R (Fig. 6a) despite smaller variations. For all experiments, the channel margins undergo a drop in effective permeability compared to background values whereas channels show a significant permeability increase (Fig. 5). The permeability difference between a channel and its side spans 5 orders of magnitude (Fig. 5a,b,c). Configuration 2 shows smaller variations but interesting results. The velocity of the main blob increases as R increases (Fig. 6b). We note that the fastest wave does not obtain maximum porosity, probably related to the aspect ratio of the blob that increases while switching from R = 10 to R = 100. The change in geometry also relates to decreased permeability on the channel walls between these two experiments, that is, effective permeability values] being smaller for the simulation with R = 100 (Fig. 5b,c).

5.3. Porosity wave as a proxy for pegmatite?

The geological application of our model considers a migmatite and a pegmatite melt to represent the porous matrix and the pore fluid from/of our numerical experiments, respectively. We further consider that the pegmatite melt behaves as a fluid because it has simple properties owing to the fact that pegmatites crystallise from a melt that does not contain a significant amount of crystals.

We define **permeability (k)** according to the experimental work of Wark and Watson (1998) that provides a permeability estimate of: $k = a^2 \varphi_0^3 / 200$ with a being the grain size. Grain sizes of ~0.01–1 mm suggest a reference permeability range of 5.10^{-15}-5.10^{-19} m^2, in agreement with measurements on crustal rocks (Achtziger-Zupančič et al., 2017; Duwiquet et al., 2019). Such grain sizes are reasonable for typical migmatite. We apply the previously defined porosity-dependent effective permeability law to scale our experiments ($k = k_0(\varphi/\varphi_0)^3$). We use the range of observed porosity values ($0.20 < \varphi < 0.45$) to calculate an effective permeability on the order 10^{-10}–10^{-16} m^2 in agreement with values reported in previous work (Connolly and Podladchikov, 2007; Keller et al., 2013; McKenzie, 1984; Schmeling et al., 2019).

The **bulk viscosity** (η) of a rock is proportional to its shear viscosity (μ_s) divided by the melt fraction with constant accounting for pore geometry. We refer the reader to the relevant literature for various expressions of bulk viscosity (Schmeling et al., 2012; Yarushina and Podladchikov, 2015). Very few direct measurements of the shear viscosity of a migmatite derive from experimental work (e.g. Arzi, 1978) On this basis Brown et al. (1995) argue that the shear viscosity μ_s of migmatite ranges between 10^{14} and 10^{17} Pa.s. We calculate a rheological law for the Westerly granite (Ji and Zhao, 1993) at different strain rates and obtain similar values for high strain rates such as modelled in metamorphic core complexes (e.g. Huet et al., 2011). We used these calculated values at temperatures in the range of 650–700 °C to estimate a reference bulk viscosity (η_0) of 10^{16} Pa.s. in agreement with previous studies (e.g. McKenzie, 1984).

We estimated several values of pegmatite **melt viscosity** (μ_f) using the model of Giordano et al. (2008) and compositions from the literature (Fig. 7). We chose the composition of the Macusani glass to be relevant for a pegmatite melt (London, 2018; London et al., 1989; Pichavant et al., 1987). We also plotted on Fig. 7 a synthetic mixture used for experimental measurements (Bartels et al., 2011) and a standard rhyolite value (Giordano et al., 2008). As discussed earlier, volatile elements have a major effect on melt viscosity, which can drop several orders of magnitude as the content of volatile elements increases. Because the equation provided by Giordano et al. (2008) does not consider all possible volatile elements that can enter a melt and act as fluxes, we calculated viscosities with water values arbitrary taken to be the loss on ignition, 5 and 10 wt% of oxides (Fig. 7). This point is supported by experimental work that reproduces pegmatite texture without any volatile component other than water (Devineau et al., 2020). We chose the interval 10^2–10^6 Pa.s to represent pegmatite melts with a preferred value of 10^4 Pa.s, which likely applies to granitic melts containing more than 5% wt% water (e.g. Dingwell et al., 1996). Melt viscosity does not change during the experiments, as stated previously for natural systems.

6. Discussion

We evaluate the implications of our results to explain the emplacement of pegmatite derived from partial melting and discuss the limitations of our modelling approach. .

6.1. Travel distances, pegmatite size, and first-order temperature considerations

Combining the results of dimensionless simulations together with geological scales of permeability and melt and bulk viscosity, we compute the timespan required for the formation of a porosity wave in our numerical experiments. The bulk rock viscosity value is set at 10^{16} Pa.s, as previously discussed. We then vary the melt viscosity values from 10^1 to 10^6 Pa.s and permeability values from 10^{-16} to 10^{-11} m^2. We calculate a possible time scale in the range 10^1–10^7 years for both configurations. It gives a wide range of possibilities. Using our preferred

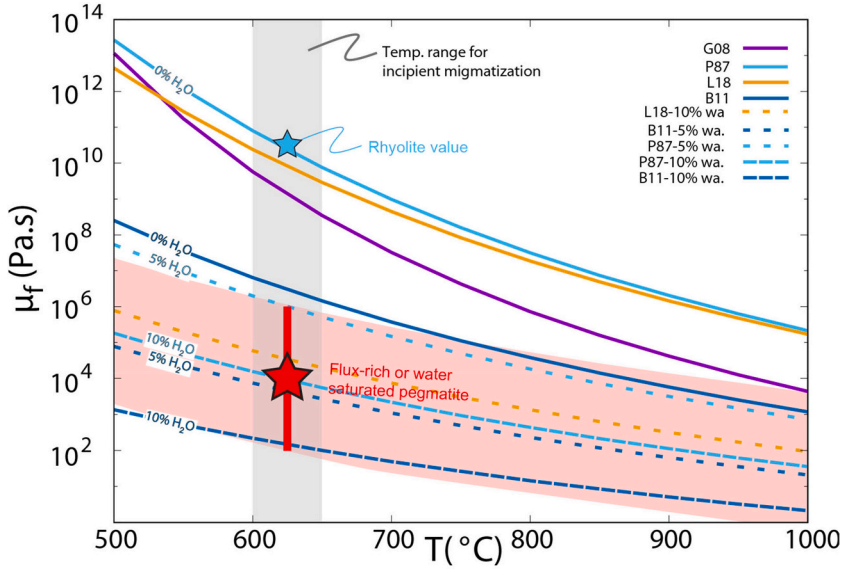

Fig. 7. Melt viscosity as a function of temperature in °C for various compositions extracted from the literature and calculated using the equation provided by Giordano et al. (2008). Plain lines correspond to original composition. Dashed lines correspond to the composition with added water. Abbreviations refer to the composition from the following authors: G08 Giordano et al. (2008); P87: Pichavant et al. (1987); L18: London, 2018; B11: Bartels et al. (2011).

magma viscosity of 10^4 Pa.s reduces the possible time span of our simulation ranges to an interval of $10^{1.5}$–$10^{5.5}$ yrs. To further reduce this interval, several reference permeability values were investigated and used to infer the travel distance of the pegmatite field (Fig. 8). The calculated travel distances range from 150 to 4800 m depending on permeability. These distances are reasonable considering the typical distance between the potential sources and the location of the pegmatite (0–6 km; Deveaud et al., 2013; London, 2018; Silva et al., 2018). For example, a permeability value of 10^{-13} m^2 allows the pegmatite to travel about 150 m and 480 m from the source in configuration 1 and configuration 2, respectively (Fig. 8a). We will discuss this point further after the introduction of a simple temperature consideration.

Pegmatite field observations and modelled channel sizes constitute a second factor to further constrain our model application. In the field, pegmatites are objects in which the melt content (i.e. the porosity) equals 100%. Their width commonly ranges from tens of centimetres to kilometres. The volume of melt-filled channels in our calculation ranges from 20 to 45% implying that either one pegmatite partially fills the channel or that numerous pegmatites are present in the channels (see inset Fig. 6a). We could thus consider that the thermal behaviour of a

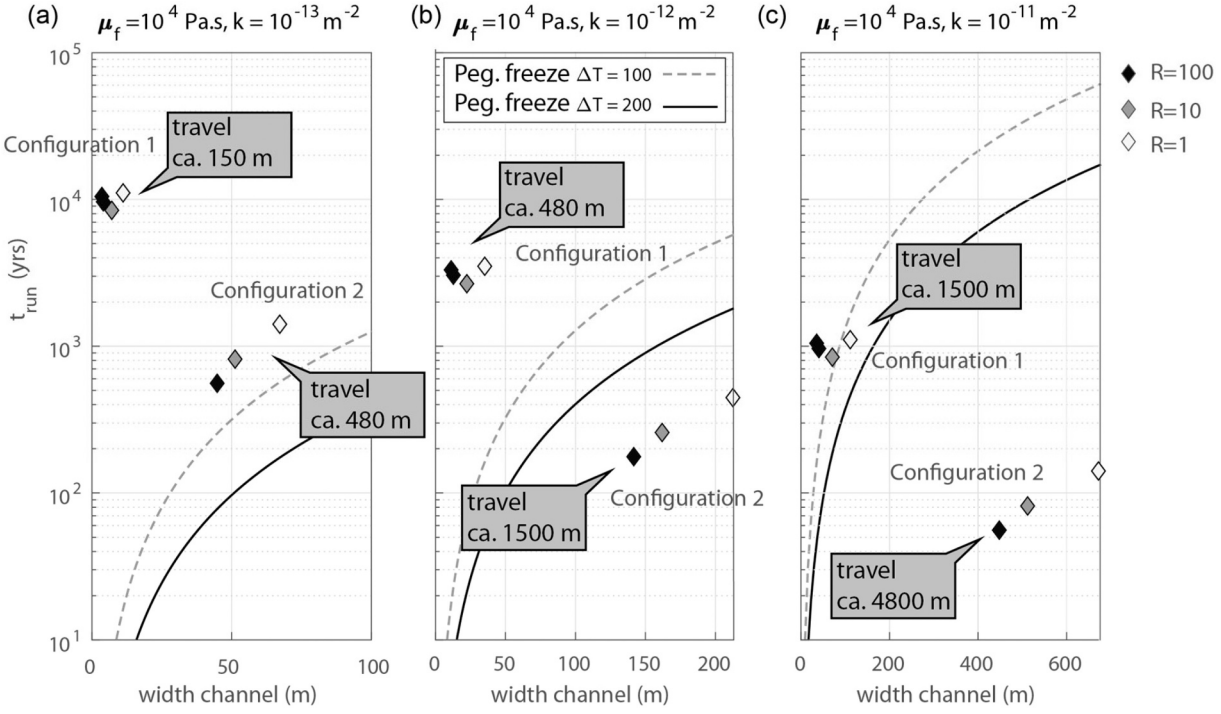

Fig. 8. Scaling of our experiments with the parameters discussed in text. Time in years (yrs) as function of the channel width in metres (m). Panels (a, b, c) depict a different value of effective permeability, 10^{-13}, 10^{-12}, 10^{-11} m^2, respectively. The dashed line corresponds to the theoretical cooling time of a dyke as discussed in the text using a first-order model (Turcotte and Schubert, 2014).

channel corresponds to that of one large dyke. We justify this statement by the diffusion length scale that we calculate to be on the order of >177 m for a simulation lasting about 1000 years ($d = \sqrt{\kappa t}$, with thermal diffusivity of $\kappa = 1.31 \times 10^{-6}$ m^2.s^{-1}; specific density $\rho = 2650$ kg.m^{-3}; heat capacity $C_p = 890$ J.kg.K^{-1}; and thermal conductivity $k = 3.1$ W.m^{-1}.K^{-1} with diffusivity κ equal to $k/[\rho\ C_p]$). This length scale is larger than most channel widths in our scaling. This scenario may not hold for configuration 2 when considering a permeability of 10^{-11} m^2 where the channels are larger than 400 m.

Temperature effects are crucial. As pegmatites crystallise from melt, the role of temperature is of the utmost importance because it helps to further constrain the application of porosity wave patterns to pegmatites. We calculate the theoretical solidification time for a dyke using a simple analytical solution (Turcotte and Schubert, 2014). We compare this analytical solution with the total duration of our simulation for three given permeability values (Fig. 8). As a first estimate, we use similar physical properties for the magma and the host rock (i.e. thermal diffusivity $\kappa = k/\rho/C_p = 1.31 \times 10^{-6}$ m^2.s^{-1} as stated previously).

Because pegmatite melt crystallises in an undercooled state ($\Delta T =$ 100–200 °C), we chose two values of 100 and 200 °C between temperatures of the magma and the host rock. We compare pegmatite travel distance to the theoretical freezing time. Considering channel width versus the analytical solution, pegmatites would freeze before reaching the top of the box in configurations 1 and 2 for a permeability of 10^{-13} m^2. Looking at Fig. 8, we see that the pegmatites can travel for a duration of only ca. 100 years according to configuration 2 and that it would freeze instantaneously for configuration 1 (Fig. 8a).

At first glance, we point out that according to the theoretical dyke-cooling model, most of the configuration 1 experiment freezes almost instantly if we do not consider strong undercooling conditions backed up by experimental crystallization experiments.

With an effective permeability of 10^{-12} m^2, pegmatites freeze quickly according to configuration 1 with a travel time < 100 years. They do not freeze before the end of the experiment in configuration 2 and they would travel at least 1500 m in approximately 100 years. Lastly, with an effective permeability of 10^{-11} m^2, some pegmatites can travel 1500 m or 4800 m depending on the undercooling value chosen for configurations 1 and 2, respectively. We note that they will/do not freeze in configuration 2 and travel at least 1500 m.

Considering a time scale of a 100 years for each simulation, all pegmatite melt bodies produced in configuration 1 freeze before the end of the simulations, whereas none of them do in configuration 2. In configuration 1, for large undercooling values, freezing can occur at distance up to 480 m for a permeability of 10^{-12} m^2 and 1500 m for a permeability of 10^{-11} m^2. In configuration 2, permeability affects the speed of the pegmatite melt body, which could travel at least 1500 m for a permeability of 10^{-12} m^2 or a minimum of 4800 m with permeability of 10^{-11} m^2.

If we consider a geothermal gradient of approximately 30 °C/km, 5 km are needed to encounter a host rock with a temperature of 500 °C. Adding that parameter to our temperature conditions, we can argue that pegmatite melts would be able to travel for all of the considered scaling.

Table 2 summarises the computed velocities for all experiments. The velocities range from a few cm/yr to tens of m/yr. These velocities are orders of magnitude lower than those inferred or calculated for volcanic systems and expected on the order of m/s (Le Gall and Pichavant, 2016; Yamato et al., 2015). This observation seems consistent with the fact that dyke systems involve a void space in which the magma percolates. The velocities however agree with the velocity computed for melt transport either in the crust or mantle (Connolly and Podladchikov, 2007; Keller et al., 2013; Keller and Katz, 2016; Schmeling et al., 2019), which are more relevant to our pegmatite application.

6.2. Comparison with field observations

In the field, pegmatites tend to cluster around fault zones when present in upper crustal levels, whereas they exhibit more scattered distributions in mid to lower crustal levels (Barros and Menuge, 2016; Deveaud et al., 2013; Gourcerol et al., 2019; Müller et al., 2015). The numerical results we present admirably reproduce the clustered and scattered behaviour observed in natural pegmatite fields. Our results suggest that pegmatite clusters will occur in more brittle environments as observed in nature (Figs. 1,4 with $R = 100$) whereas scattered pegmatites will occur in more viscous environments, which are generally associated in the field with warm settings, such as migmatite domes, or the mid to lower crust (Figs. 1,4,5; with R = 1).

Our model results further suggest that pegmatites will travel greater distances in environments with higher effective permeability. This observation confirms the analogy to fault zones in natural environments that feature a large background permeability increase. Our assumption of effective permeability values as high as 10^{-11} m^2 are supported by measurements of damaged rock zones (Achtziger-Zupančič et al., 2017; Duwiquet et al., 2019). Our experiments show dynamic permeability variations of about 5 orders of magnitude between the very high permeability channel interior and its low permeability margins or walls (Figs. 4,5).

We interpreted this behaviour as the opening of fluid or melt pathways that seal shortly after passage of a porosity wave (Figs. 2b,4,5). Such pathways efficiently transport melt over large distances, hundreds of metres to several kilometres according to our calculation. In the field, it is difficult to identify the passage of a pervasive melt flow due to the thermal regime of the mid to lower crustal environment and to the transient nature of the melt flow. Melt formed during partial melting collects and escapes its initial emplacement after reaching the melt percolation threshold (e.g. Brown, 2013 and references therein). It then travels to a place where it freezes. The first and terminal steps are often observed (e.g. migmatite, pegmatite, granite). However, intermediate steps are transient by nature whereas the geological record is usually post mortem and is hardly capable of capturing transport. The record of such melt pathways has been proposed in the lower crust (Stuart et al., 2016; Stuart et al., 2018) and in ophiolites (e.g. Kelemen et al., 1995). The pathway evidence is also suggested when aqueous fluids are involved (e.g. Plümper et al., 2016).

We highlight the importance of hydrothermal inheritance (reuse) that we observe in our experiments. We systematically observe (i) residual transient high permeability patterns where the porosity wave has travelled and (ii) secondary waves migrating in existing channels. Figs. 4b and c capture this behaviour as secondary waves join pre-existing pathways. We also observe that secondary waves that are developing on their own are being caught by inherited channels of former waves of greater magnitude (Fig. 4c). This observation is important as it may help to explain pegmatite distribution and pegmatite field orientations that generally show similar elongation (Deveaud et al., 2013; Silva et al., 2018). In addition, an open question remains

Table 2
Summary of the scaled velocity of the pegmatite-forming melt.

		Configuration 1				Configuration 2		
k (m^2)	v (m/yr)	R = 1	R = 10	R = 100	R = 100 / Var Mus	R = 1	R = 10	R = 100
$k = 10^{-11}$	v (m/yr)	1.37	1.8	1.76	1.45	34	58.8	85.89
$k = 10^{-12}$	v (m/yr)	0.137	0.18	0.176	0.145	3.4	5.88	8.589
$k = 10^{-13}$	v (m/yr)	0.0137	0.018	0.0176	0.0145	0.34	0.588	0.8589

regarding the time and temperature needed to heal the crust after melt circulation; specifically, warmer mid and lower crustal environments may promote faster pathway healing compared to upper crustal levels, for which complete pathway healing is unlikely. We believe these considerations help explain the regular pegmatite distribution in warm environments such as migmatitic domes. In upper crustal levels, pathways for pegmatite ascent may even predate melt circulation considering the ubiquitous presence of faults and other fluid pathways that pegmatites make use of.

As stated by Brown (2013), and to further validate the application of porosity waves to melt transport in the crust, we need more field data. Additional data such as the spacing between melt flow structures and their sizes could be compared with two-phase flow model results to evaluate/determine if the rheological and hydromechanical properties considered by the models match the observations. These data are partially available from the field (Deveaud et al., 2013; Silva et al., 2018), partially from our numerical study, and also from previous studies (e.g. Räss et al., 2019). Our study proposes a first-order comparison with available statistical data. We chose configuration 1 with R = 100 to perform this comparison because it shows multiple channels. We compared it with the Ambazac and the Barroso-Alvão pegmatite fields (Deveaud et al., 2013; Silva et al., 2018) that are the only ones where spatial statistical field data are available on the pegmatites distribution. The Ambazac pegmatite field belongs to a larger rare metal magmatic belt located on the northern edge of the Variscan Central Massif in France. The most differentiated pegmatites emplaced around 310 Ma (Deveaud et al., 2013 and references therein). These pegmatite swarm intrudes mainly the Saint Sylvestre Granitic complex that formed at ca. 324 Ma. Both the age difference and statistical field relation point to the lack of relation between the granites and the pegmatites. The Barroso-Alvão pegmatitic field is located in the Tràs-os-Montes region of Portugal, belonging to the Variscan Ibero-Armorican arc. The pegmatite are mainly found in the parautochtonous terrain, made of the amphibolite-facies meta-sedimentary rocks. Statistical method emphasize the absence of spatial emplacement relationship between the pegmatite and surrounding granitic bodies (Silva et al., 2018). Both area represent pegmatites that are emplaced at mid crustal levels and along fault zones.

The field statistical approach shows that in the Ambazac region, the distance between a pegmatite and its nearest neighbour is 528 m with a median distance of 367 m. We note that more than 50% of the population is distributed in the 0–400 m bin. In the Barroso-Alvão district, the average distance to the nearest neighbour is 143 m and the 50–100 m bin contains more than 35% of the population. These distances are compatible with the 40 to 200 m spacing in our experiment for a reference permeability of 10^{-11} m^2, which most likely corresponds to crustal environments where fault zones are present (e.g. Duwiquet et al., 2019). Distances between pegmatites range from 64 to 12 m for permeability values of 10^{-12} m^2. These distances are consistent with what is observed in the Barroso-Alvão district where the minimum distance between pegmatites is ca. 5 m. Additional data on field where pegmatite show a deeper emplacement level (e.g. in the Scveconorwegian orogeny; Müller et al., 2017) would constitute an ideal case study to explore the distribution of pegmatites in mid to lower crustal rocks. Performing a full data inversion of the models and a comparison with field observations would promote a better understanding of melt migration in the crust. However, the level at which we compare the model and field observations remains a critical parameter as we cannot ensure that pegmatites observed in the field strictly represent the same geological events.

A last point of discussion concern the specific case of rare metal bearing pegmatites. There are many places, amongst other: the Moldanubian domain of the Bohemian massif in Czech Republic, the Sveconorwegian pegmatite province of Norway and Sweeden, the Lewisian gneiss complex of Scotland, the Maine pegmatite province) where granitic pegmatites coexist with rare metal pegmatite (Melleton et al., 2012; Müller et al., 2017; Shaw et al., 2016; Webber et al., 2019).

Our models agree well with the coexistence of pegmatites with different chemistry. We can first consider the possibility of differences in the chemistry of the protolith (e.g. meta-evaporitic layers interbedded in meta-pelitic would be an extreme but favourable case; e.g. Simmons and Webber, 2008). The difference of chemistry in the anatectic domain would simply correspond to the coexistence of pegmatites with different chemistry along the horizontal axis. In addition, if we consider that the rare metal enriched melt would escape first upon the breakdown of a rare metal carrier (e.g. Li in staurolite; Chopin et al., 2003; Konzett et al., 2018). This first batch of enriched melt will be followed by a "normal" granitic melt after the consumption of all the rare metal carrier. This can be seen of Figs. 4b,c,d, and to a less extent on Figs. 5b,c, that show models where a first wave of pegmatite escape the source. The pegmatites are followed by another train of pegmatites escaping the same anatectic area. This case would correspond the coexistence of rare metal enriched pegmatites (the first ones) and to barren granitic pegmatites (the "followers"). A mixture of both hypothesis is certainly the best answer we can provide to explain the spatial relation of rare metal bearing and barren pegmatite in the area previously mentioned.

6.3. Limitation of the model

"All models are wrong, but some are useful" (Box, 1979) highlights our awareness about the limitations of our simple model compared to the vast complexity of natural objects such as pegmatites.

Amongst the modelling parameter, we considered a constant background viscosity value. This is realistic at first order only if we do not consider that the pegmatite travel more than a few kilometres. We tested a case with variations in the background shear viscosity. It does not affect significantly the general pattern (Fig. 4c,d). An intrinsic simplification of our modelling approach is to consider the background of the porous media to contain 1% of porosity, corresponding to 1% of melt. This is non-realistic, for higher crustal levels. Because the porosity waves do not collect porosity from the surroundings after it escapes the initial anomaly, this assumption is not important and does not affect our calculation. The variation in the value of the initial porosity anomaly is not critical since porosity form for at any value $<10\%$ (and larger than the reference porosity of 1%; see e.g. Connolly and Podladchikov, 2007; Räss et al., 2019). Lower values for the initial anomaly have minor effects on the general pattern of the wave. They however have important effect on the maximum amount of porosity that can be collected. Higher value (i.e. higher that the melt percolation threshold) for the initial anomaly do not apply to incipient partial melting and were not considered.

In our model, we considered a constant fluid viscosity. This applies well to granitic pegmatite or to rare metal pegmatites if we do not consider their coexistence. However if they coexist, we can expect a difference in their viscosity. This difference might not be so important considering that the first batch of melting would occur in an environment rich in flux elements whereas the subsequent melting batches would occur with higher water quantities but minor quantities of other volatile elements (e.g. Li, B, P, F). Therefore the viscosity of both melts could be similar or at least within the same order of magnitude (Fig. 7).

The first-order thermal considerations we hypothesise may represent a limiting factor but facilitate an assessment of how much time and how much distance pegmatites can travel in a homogenous viscous crust. A second limiting assumption is the constant background viscosity values that we consider, although variations in background shear viscosity do not seem to significantly affect the general pattern (Fig. 4d). However, since most rheological laws are temperature dependent, we may need to include diffusive and advective thermal processes and consider their couplings to the hydromechanical processes predicted by our model. This next step may make it possible to further investigate the pegmatite problem with the same detail as for melt circulation in the crust or mantle (e.g. Keller and Katz, 2016; Schmeling et al., 2019).

7. Conclusions

By applying our porosity wave models to pegmatites, we show that (i) it is theoretically possible to transport pegmatite melt originating from a source with a low amount of melting (i.e. partial melting of ca. 10%). In nature that environment would correspond to a migmatite. Our model supports the hypothesis that some pegmatites can originate from partial melting (the Stewart model). Our application also shows (ii) the interpretation of pegmatites as an expression of spontaneous crustal flow localization and shows that the porosity wave approach reproduces first-order scattered versus clustered distributions observed in pegmatite fields. This distribution reflects the level of emplacement in the crust (deep versus shallow). We also show (iii) that the porosity wave mechanism allows the transport of a pegmatitic melt relatively far from its source (up to a few kilometres). Also, this fluid-focused mechanism does not require the existence of a short-lived but infinite magma supply that may exist only in a volcanic system (Harris et al., 2000; Petford et al., 1993) or in the immediate vicinity of a granitic body. To date, this had been the only possible driving mechanism postulated for pegmatite transport (Baker, 1998; Rubin, 1995). We also conclude (iv) that transport in wide channels (>400 m) or narrow channels (few metres) is fairly rapid (<100–1000 yr) and is consistent with estimates based upon chemical data for granitic rocks (Harris et al., 2000). The rapid transit also agrees with the short timescale of pegmatite cooling (Phelps et al., 2020). Note that this last point has not yet been addressed in the literature. The scaling we present here may also apply well to granitic melt produced during anatexis; therefore our results suggest that the porosity wave may be an efficient mechanism for transporting melt in the crust, as already suggested (Bouilhol et al., 2011; Brown, 2013). An approach similar to the one we suggest may well explain the genesis of S-type granites (or some granitoids) by successive melting events, as recorded by natural data (Clemens and Stevens, 2016).

Declaration of Competing Interest

The authors declare that they have no known competing financial interests or personal relationships that could have appeared to influence the work reported in this paper.

Acknowledgements

This research was funded through the ANR VARPEG (ANR15-CE01-0001) granted to M. Pichavant and the LABEX VOLTAIRE (ANR-10-LABX-100-01). AP thanks the L. Guillou-Frottier and VARPEG team for discussion. Prolific interaction with L. van Unik Hoorn greatly helped AP during the preparation of this manuscript. We thank the four anonymous reviewers for constructive comments. The manuscript benefited from revision by P. Bobeck (DBA Geotechnical Translations).

References

Achtziger-Zupančič, P., Loew, S., Mariéthoz, G., 2017. A new global database to improve predictions of permeability distribution in crystalline rocks at site scale. J. Geophys. Res. Solid Earth 122, 3513–3539. https://doi.org/10.1002/2017JB014106.

Arzi, A.A., 1978. Critical phenomena melted rocks in the rheology of partially. Tectonophysics 44, 173–184.

Baker, D.R., 1998. The escape of pegmatite dikes from granitic plutons: Constraints from new models of viscosity and dike propagation. Can. Mineral. 36, 255–263.

Barros, R., Menuge, J., 2016. The origin of spodumene pegmatites associated with the leinster granite in Southeast Ireland. Can. Mineral. 54, 847–862. https://doi.org/10.3749/canmin.1600027.

Bartels, A., Vetere, F., Holtz, F., Behrens, H., Linnen, R.L., 2011. Viscosity of flux-rich pegmatitic melts. Contrib. Mineral. Petrol. 162, 51–60. https://doi.org/10.1007/s00410-010-0582-3.

Bartels, A., Behrens, H., Holtz, F., Schmidt, B.C., Fechtelkord, M., Knipping, J., Crede, L., Baasner, A., Pukallus, N., 2013. The effect of fluorine, boron and phosphorus on the viscosity of pegmatite forming melts. Chem. Geol. 346, 184–198. https://doi.org/10.1016/j.chemgeo.2012.09.024.

Bartels, A., Behrens, H., Holtz, F., Schmidt, B.C., 2015. The effect of lithium on the viscosity of pegmatite forming liquids. Chem. Geol. 410, 1–11. https://doi.org/10.1016/j.chemgeo.2015.05.011.

Bouilhol, P., Connolly, J.A.D., Burg, J.P., 2011. Geological evidence and modeling of melt migration by porosity waves in the sub-arc mantle of Kohistan (Pakistan). Geology 39, 1091–1094. https://doi.org/10.1130/G32219.1.

Box, G.E., 1979. Robustness in the strategy of Scientific Model Building. In: Robustness in Statistics. Elsevier, pp. 201–236. https://doi.org/10.1016/B978-0-12-438150-6.50018-2.

Brown, M., 2013. Granite: from genesis to emplacement. Geol. Soc. Am. Bull. 125, 1079–1113. https://doi.org/10.1130/B30877.1.

Brown, M., Averkin, Y.A., McLellan, E.L., Sawyer, E.W., 1995. Melt segregation in migmatites. J. Geophys. Res. 100, 15655. https://doi.org/10.1029/95JB00517.

Cameron, E.N., Jahns, R.H., McNair, A.H., Page, L.R., 1949. Int. Struct. Granitic Pegmatites. https://doi.org/10.5382/MONO.02.

Černý, P., Ercit, T.S., 2005. The classification of granitic pegmatites revisited. Can. Mineral. 43, 2005–2026. https://doi.org/10.2113/gscanmin.43.6.2005.

Černý, P., Blevin, P., Cuney, M., London, D., 2005. Granite-related ore deposits. Econ. Geol. 100, 337–370.

Chakoumakos, B.C., Lumpkin, G.R., 1990. Pressure-temperature constraints on the crystallization of the Harding pegmatite, Taos county, New Mexico. Can. Mineral. 28, 287–298.

Chopin, C., Goffe, B., Ungaretti, L., Oberti, R., 2003. Magnesiostaurolite and zincostaurolite: mineral description with a petrogenetic and crystal-chemical update. Eur. J. Mineral. 15, 167–176. https://doi.org/10.1127/0935-1221/2003/0015-0167.

Clemens, J.D., Stevens, G., 2016. Melt segregation and magma interactions during crustal melting: breaking out of the matrix. Earth-Science Rev. 160, 333–349. https://doi.org/10.1016/j.earscirev.2016.07.012.

Connolly, J.A.D., Podladchikov, Y.Y., 2007. Decompaction weakening and channeling instability in ductile porous media: Implications for asthenospheric melt segregation. J. Geophys. Res. Solid Earth 112, 1–15. https://doi.org/10.1029/2005JB004213.

Connolly, J.A.D., Podladchikov, Y.Y., 2015. An analytical solution for solitary porosity waves: dynamic permeability and fluidization of nonlinear viscous and viscoplastic rock. GeoFluids 15, 269–292. https://doi.org/10.1002/9781119166573.ch23.

Costa, A., 2006. Permeability-porosity relationship: a reexamination of the Kozeny-Carman equation based on a fractal pore-space geometry assumption. Geophys. Res. Lett. 33, L02318. https://doi.org/10.1029/2005GL025134.

Demartis, M., Pinotti, L.P., Coniglio, J.E., D'Eramo, F.J., Tubía, J.M., Aragón, E., Agulleiro Insúa, L.A., 2011. Ascent and emplacement of pegmatitic melts in a major reverse shear zone (Sierras de Córdoba, Argentina). J. Struct. Geol. 33, 1334–1346. https://doi.org/10.1016/j.jsg.2011.06.008.

Deubelbeiss, Y., Kaus, B.J.P., Connolly, J.A.D., Caricchi, L., 2011. Potential causes for the non-Newtonian rheology of crystal-bearing magmas. Geochemistry Geophys. Geosystems 12, 1–22. https://doi.org/10.1029/2010GC003485.

Deveaud, S., Gumiaux, C., Gloaguen, E., Branquet, Y., 2013. Spatial statistical analysis applied to rare-element LCT-type pegmatite felds: an original approach to constrain faults-pegmatites-granites relationships. J. Geosci. (Czech Republic) 58, 163–182. https://doi.org/10.3190/jgeosci.141.

Deveaud, S., Guillou-frottier, L., Millot, R., Gloaguen, E., Branquet, Y., Villaros, A., Pichavant, M., Silva, D., Deveaud, S., Guillou-frottier, L., Millot, R., Gloaguen, E., Branquet, Y., 2015. Innovative and Multi-Disciplinary Approach for Discussing the Emplacement of Variscan LCT-Pegmatite Fields.

Devineau, K., Champallier, R., Pichavant, M., 2020. Dynamic crystallization of a haplogranitic melt - application to pegmatites. J. Petrol. https://doi.org/10.1093/petrology/egaa054.

Dingwell, D.B., Hess, K., Knoche, R., 1996. Granite and granitic pegmatite melts : volumes and viscosities. Trans. R. Soc. Edinb. Earth Sci. 87, 65–72.

Duwiquet, H., Arbaret, L., Guillou-Frottier, L., Heap, M.J., Bellanger, M., 2019. On the geothermal potential of crustal fault zones: a case study from the Pontgibaud area (French Massif Central, France). Geotherm. Energy 7. https://doi.org/10.1186/s40517-019-0150-7.

Fei, G., Menuge, J.F., Li, Y., Yang, J., Deng, Y., Chen, C., Yang, Y., Yang, Z., Qin, L., Zheng, L., Tang, W., 2020. Petrogenesis of the Lijiagou spodumene pegmatites in Songpan-Garze Fold Belt, West Sichuan, China: evidence from geochemistry, zircon, cassiterite and coltan U-Pb geochronology and Hf isotopic compositions. Lithos 364–365, 105555. https://doi.org/10.1016/j.lithos.2020.105555.

Giordano, D., Russell, J.K., Dingwell, D.B., 2008. Viscosity of magmatic liquids: a model. Earth Planet. Sci. Lett. 271, 123–134. https://doi.org/10.1016/j.epsl.2008.03.038.

Gourcerol, B., Gloaguen, E., Melleton, J., Tuduri, J., Galiegue, X., 2019. Re-assessing the European lithium resource potential – a review of hard-rock resources and metallogeny. Ore Geol. Rev. 109, 494–519. https://doi.org/10.1016/j.oregeorev.2019.04.015.

Harris, N., Vance, D., Ayres, M., 2000. From sediment to granite: Timescales of anatexis in the upper crust. Chem. Geol. 162, 155–167. https://doi.org/10.1016/S0009-2541(99)00121-7.

Hiscock, K., Bense, V.F., 2014. Hydrogeology: Principles and Practice, 2nd ed. Wiley-Blackwell.

Huet, B., Le Pourhiet, L., Labrousse, L., Burov, E.B., Jolivet, L., 2011. Formation of metamorphic core complex in inherited wedges: a thermomechanical modelling study. Earth Planet. Sci. Lett. 309, 249–257. https://doi.org/10.1016/j.epsl.2011.07.004.

Ji, S., Zhao, P., 1993. Flow laws of multiphase rocks calculated from experimental data on the constituent phases. Earth Planet. Sci. Lett. 117, 181–187. https://doi.org/10.1016/0012-821X(93)90125-S.

Kelemen, P.B., Shimizu, N., Salters, V., 1995. Extraction of mid-ocean-ridge basalt from the upwelling mantle.Pdf. Nature 375, 747–753.
Keller, T., Katz, R.F., 2016. The Role of Volatiles in Reactive Melt Transport in the Asthenosphere. J. Petrol. 57, 1073–1108. https://doi.org/10.1093/petrology/egw030.
Keller, T., May, D.A., Kaus, B.J.P., 2013. Numerical modelling of magma dynamics coupled to tectonic deformation of lithosphere and crust. Geophys. J. Int. 195, 1406–1442. https://doi.org/10.1093/gji/ggt306.
Konzett, J., Hauzenberger, C., Ludwig, T., Stalder, R., 2018. Anatectic granitic pegmatites from the eastern alps: a case of variable rare metal enrichment during high-grade regional metamorphism. II: Pegmatite staurolite as an indicator of anatectic pegmatite parent melt formation - a field and experimental study. Can. Mineral. 56, 603–624. https://doi.org/10.3749/canmin.1800011.
Le Gall, N., Pichavant, M., 2016. Experimental simulation of bubble nucleation and magma ascent in basaltic systems: Implications for Stromboli volcano. Am. Mineral. 101, 1967–1985. https://doi.org/10.2138/am-2016-5639.
London, D., 2014. A petrologic assessment of internal zonation in granitic pegmatites. Lithos 184–187, 74–104. https://doi.org/10.1016/j.lithos.2013.10.025.
London, D., 2015. Reply to Thomas and Davidson on “a petrologic assessment of internal zonation in granitic pegmatites” (London, 2014a). Lithos 212–215, 469–484. https://doi.org/10.1016/j.lithos.2014.11.025.
London, D., 2018. Ore-forming processes within granitic pegmatites. Ore Geol. Rev. 101, 349–383. https://doi.org/10.1016/j.oregeorev.2018.04.020.
London, D., Morgan, G.B., 2017. Experimental Crystallization of the Macusani Obsidian, with applications to Lithium-rich Granitic Pegmatites. J. Petrol. 58, 1005–1030. https://doi.org/10.1093/petrology/egx044.
London, D., Morgan, G.B., Hervig, R.L., 1989. Vapor-undersaturated experiments with Macusani glass+H2O at 200 MPa, and the internal differentiation of granitic pegmatites. Contrib. Mineral. Petrol. 102, 1–17. https://doi.org/10.1007/BF01160186.
McKenzie, D., 1984. The Generation and Compaction of Partially Molten Rock. J. Petrol. 25, 713–765.
Melleton, J., Gloaguen, E., Frei, D., Novák, M., Breiter, K., 2012. How are the emplacement of rare-element pegmatites, regional metamorphism and magmatism interrelated in the Moldanubian domain of the Variscan Bohemian Massif, Czech Republic? Can. Mineral. 50, 1751–1773. https://doi.org/10.3749/canmin.50.6.1751.
Müller, A., Ihlen, P.M., Snook, B., Larsen, R.B., Flem, B., Bingen, B., Williamson, B.J., 2015. The chemistry of quartz in granitic pegmatites of southern Norway: Petrogenetic and economic implications. Econ. Geol. 110, 1737–1757. https://doi.org/10.2113/econgeo.110.7.1737.
Müller, A., Romer, R.L., Pedersen, R.B., 2017. The sveconorwegian pegmatite province -thousands of pegmatites without parental granites. Can. Mineral. 55, 283–315. https://doi.org/10.3749/canmin.1600075.
Myers, M.L., Wallace, P.J., Wilson, C.J.N., 2019. Inferring magma ascent timescales and reconstructing conduit processes in explosive rhyolitic eruptions using diffusive losses of hydrogen from melt inclusions. J. Volcanol. Geotherm. Res. 369, 95–112. https://doi.org/10.1016/j.jvolgeores.2018.11.009.
Petford, N., Kerr, R.C., Lister, J.R., 1993. Dike transport of granitoid magmas. Geology 21, 845–848. https://doi.org/10.1130/0091-7613(1993)021<0845:DTOGM>2.3.CO;2.
Phelps, P.R., Lee, C.T.A., Morton, D.M., 2020. Episodes of fast crystal growth in pegmatites. Nat. Commun. 11 https://doi.org/10.1038/s41467-020-18806-w.
Pichavant, M., Herrera, J.V., Boulmier, S., Briqueu, L., Joron, J.L., Juteau, M., Marin, L., Michard, A., Shepard, S.M.F., Treuil, M., Vernet, M., 1987. The Macusani glasses, SE Peru: evidence of chemical fractionation in peraluminous magmas. Geochem. Soc. Spec. Publ. 1, 359–373.
Plümper, O., John, T., Podladchikov, Y.Y., Vrijmoed, J.C., Scambelluri, M., 2016. Fluid escape from subduction zones controlled by channel-forming reactive porosity. Nat. Geosci. 10, 150–156. https://doi.org/10.1038/ngeo2865.
Räss, L., Simon, N.S.C., Podladchikov, Y.Y., 2018. Spontaneous formation of fluid escape pipes from subsurface reservoirs. Sci. Rep. 8, 11116. https://doi.org/10.1038/s41598-018-29485-5.
Räss, L., Duretz, T., Podladchikov, Y.Y., 2019. Resolving hydromechanical coupling in two and three dimensions: spontaneous channelling of porous fluids owing to decompaction weakening. Geophys. J. Int. 218, 1591–1616. https://doi.org/10.1093/gji/ggz239.
Rubin, A.M., 1995. Getting granite dikes out of the source region. J. Geophys. Res. Solid Earth 100, 5911–5929. https://doi.org/10.1029/94JB02942.
Rubin, A.M., 1998. Dike ascent in partially molten rock. J. Geophys. Res. 103 https://doi.org/10.1029/2001JD900007.
Schmeling, H., Kruse, J.P., Richard, G., 2012. Effective shear and bulk viscosity of partially molten rock based on elastic moduli theory of a fluid filled poroelastic medium. Geophys. J. Int. 190, 1571–1578. https://doi.org/10.1111/j.1365-246X.2012.05596.x.
Schmeling, H., Marquart, G., Weinberg, R., Wallner, H., 2019. Modelling melting and melt segregation by two-phase flow: New insights into the dynamics of magmatic systems in the continental crust. Geophys. J. Int. 217, 422–450. https://doi.org/10.1093/gji/ggz029.
Scott, D.R., Stevenson, D.J., 1984. Magma solitons. Geophys. Res. Lett. 11, 1161–1164. https://doi.org/10.1029/GL011i011p01161.
Shaw, R.A., Goodenough, K.M., Roberts, N.M.W., Horstwood, M.S.A., Chenery, S.R., Gunn, A.G., 2016. Petrogenesis of rare-metal pegmatites in high-grade metamorphic terranes: a case study from the Lewisian Gneiss complex of north-West Scotland. Precambrian Res. 281, 338–362. https://doi.org/10.1016/j.precamres.2016.06.008.
Silva, D., Lima, A., Gloaguen, E., Gumiaux, C., Noronha, F., Deveaud, S., 2018. spatial geostatistical analysis applied to the Barroso-Alvão Rare-elements Pegmatite Field (Northern Portugal). Front. Informat. Syst. https://doi.org/10.2174/97816810861181180100006.
Simmons, W.B.S., Webber, K.L., 2008. Pegmatite genesis: state of the art. Eur. J. Mineral. 20, 421–438. https://doi.org/10.1127/0935-1221/2008/0020-1833.
Simmons, W., Falster, A., Webber, K., Roda-Robles, E., Boudreaux, A.P., Grassi, L.R., Freeman, G., 2016. Bulk composition of MT. Mica Pegmatite, Maine, USA: Implications for the Origin of an LCT Type Pegmatite by Anatexis. Can. Mineral. 54, 1053–1070. https://doi.org/10.3749/canmin.1600017.
Stewart, D.B., 1978. Petrogenesis of lithium-rich pegmatites. Am. Mineral. 63, 970–980, 0003-004X/78/0910-0970$02.00.
Stuart, C.A., Piazolo, S., Daczko, N.R., 2016. Mass transfer in the lower crust. Geochemistry. Geophys. Geosystems 17, 3733–3753. https://doi.org/10.1002/2015GC006236.Received.
Stuart, C.A., Piazolo, S., Daczko, N.R., 2018. The recognition of former melt flux through high-strain zones. J. Metamorph. Geol. 36, 1049–1069. https://doi.org/10.1111/jmg.12427.
Thomas, R., Davidson, P., 2012. Water in granite and pegmatite-forming melts. Ore Geol. Rev. 46, 32–46. https://doi.org/10.1016/j.oregeorev.2012.02.006.
Turcotte, D.L., Schubert, G., 2014. Geodynamics, 3rd ed. Cambridge University Press.
Wark, D., Watson, E.B., 1998. Grain-scale permeabilities of texturally equilibrated , monomineralic rocks. Earth Planet. Sci. Lett. 164, 591–605.
Webber, K.L., Simmons, W.B., Falster, A.U., Hanson, S.L., 2019. Anatectic pegmatites of the Oxford County pegmatite field, Maine. USA. Can. Mineral. 57, 811–815. https://doi.org/10.3749/canmin.AB00028.
Yamato, P., Duretz, T., May, D.A., Tartèse, R., 2015. Quantifying magma segregation in dykes. Tectonophysics 660, 132–147. https://doi.org/10.1016/j.tecto.2015.08.030.
Yarushina, V.M., Podladchikov, Y.Y., 2015. (De)compaction of porous viscoelastoplastic media: Model formulation. J. Geophys. Res. Solid Earth 120, 4146–4170. https://doi.org/10.1002/2014JB011258.Received.
Yarushina, V.M., Podladchikov, Y.Y., Connolly, J.A.D., 2015. (De)compaction of porous viscoelastoplastic media: Solitary porosity waves. J. Geophys. Res. Solid Earth 1–20. https://doi.org/10.1002/2014JB011260.Received.